J. Fluid Mech. (2023), *vol*. 971, A34, doi:10.1017/jfm.2023.685

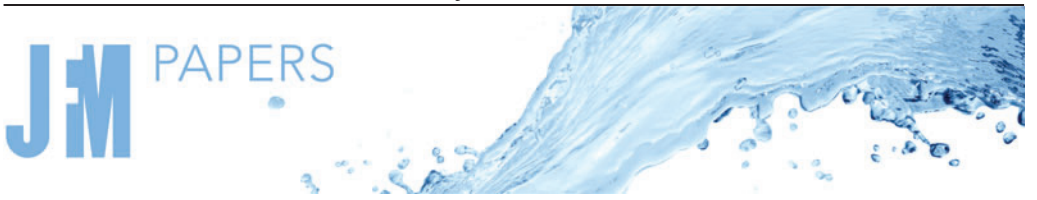

Coalescence of immiscible sessile droplets on a partial wetting surface

Huadan Xu[1], **Xinjin Ge**[1], **Tianyou Wang**[1] **and Zhizhao Che**[1],†

[1]State Key Laboratory of Engines, Tianjin University, Tianjin 300350, PR China

(Received 10 May 2023; revised 14 July 2023; accepted 14 August 2023)

Droplet coalescence is a common phenomenon and plays an important role in multidisciplinary applications. Previous studies mainly consider the coalescence of miscible liquids, even though the coalescence of immiscible droplets on a solid surface is a common process. In this study, we explore the coalescence of two immiscible droplets on a partial wetting surface experimentally and theoretically. We find that the coalescence process can be divided into three stages based on the time scales and force interactions involved, namely (I) the growth of a liquid bridge, (II) the oscillation of the coalescing sessile droplet and (III) the formation of a partially engulfed compound sessile droplet and the subsequent retraction. In stage I, the immiscible interface is found not to affect the scaling of the temporal evolution of the liquid bridge, which follows the same 2/3 power law as that of miscible droplets. In stage II, by developing a new capillary time scale considering both surface and interfacial tensions, we show that the interfacial tension between the two immiscible liquids functions as a non-negligible resistance to the oscillation which decreases the oscillation periods. In stage III, a modified Ohnesorge number is developed to characterize the visco-capillary and inertia-capillary time scales involved during the displacement of water by oil; a new model based on energy balance is proposed to analyse the maximum retraction velocity, highlighting that the viscous resistance is concentrated in a region close to the contact line.

Key words: breakup/coalescence, drops

1. Introduction

Droplet coalescence has long been an important research topic and has attracted growing interest due to its close relevance to broad applications such as material synthesis (Song, Chen & Ismagilov 2006; Sohrabi, Kassir & Keshavarz Moraveji 2020), aircraft anti-icing (Cha *et al.* 2016; Kamp, Villwock & Kraume 2017) and efficient cooling (Gong, Gao

† Email address for correspondence: chezhizhao@tju.edu.cn

& Jiang 2017; Wang *et al.* 2022). Most of the previous studies of droplet coalescence considered the coalescence of two spherical droplets (Duchemin, Eggers & Josserand 2003; Thoroddsen *et al.* 2007; Paulsen 2013). The coalescence dynamics of two sessile droplets (i.e. liquid droplets sitting on solid substrates), in comparison, is inherently different due to the presence of a solid substrate (Hernandez-Sanchez *et al.* 2012; Eddi, Winkels & Snoeijer 2013; Sui *et al.* 2013; Pawar *et al.* 2019*b*). Considering its great importance in applications in digital microfluidics (Choi *et al.* 2012), precise control of inkjet printing (Lee *et al.* 2013) and dropwise condensation (Wang *et al.* 2022), the coalescence of sessile droplets continues to be an active area of research. The coalescence of sessile droplets can be strongly affected due to the interaction with solid surfaces (Neogi & Miller 1982). Due to the extra resistance from the solid surfaces, the coalescence of sessile droplets consists of other different dynamics, such as oscillation (Somwanshi, Muralidhar & Khandekar 2018; Jiang, Zhao & Chen 2019) and contact line relaxation (Gokhale *et al.* 2004; Beysens & Narhe 2006).

When two spherical droplets are made to touch and coalesce, a small liquid bridge forms connecting the two droplets driven by capillary forces (Aarts *et al.* 2005; Thoroddsen *et al.* 2007; Xu, Wang & Che 2022). Then, depending on the competition between inertia and viscous forces, the radius of the liquid bridge r grows as $r \sim t$ (if viscous force is the dominant resistance) or as $r \sim t^{1/2}$ (if inertia is the dominant resistance), with a crossover length depending on the size of the droplets and fluid properties (Paulsen 2013). However, the bridge dynamics of two sessile droplets could show radically different behaviours compared with that of two spherical droplets due to the different geometries caused by the presence of substrate. Recently, the influence of geometry (the initial shape of the droplet before coalescence) on the coalescence dynamics was investigated. The short-time dynamics of droplet coalescence on solid surfaces can be characterized by the liquid bridge evolution (Eddi *et al.* 2013; Sui *et al.* 2013; Pawar *et al.* 2019*b*) and the growth of the bridge height (h_m) follows a power law: $h_m \sim t^{\alpha}$. For viscous droplets on a partial wetting surface, the time evolution of the liquid bridge was found to grow linearly with time (i.e. $\alpha = 1$), where the droplet was introduced by either liquid deposition or vapour condensation (Narhe, Beysens & Pomeau 2008; Hernandez-Sanchez *et al.* 2012). In another relevant study where silicone oil droplets were put on a perfectly wetting substrate, the droplet height and radius before the contact were demonstrated to have a large influence on the growth rate of the liquid bridge (Ristenpart *et al.* 2006). Lee *et al.* (2013) conducted an experiment on wettable surfaces with contact angles ranging from 10° to 56° using an electrohydrodynamic inkjet system and obtained a power-law exponent of $0.51 \leqslant \alpha \leqslant 0.86$. In another investigation by Eddi *et al.* (2013) using two equal-sized water droplets, they discovered that the liquid bridge dynamics is related to the initial shape of the droplet, following an exponent of 2/3 for a contact angle smaller than 90° and an exponent of 1/2 when the contact angle approaches 90° (Eddi *et al.* 2013).

After the completion of liquid bridge growth, there follows a slower process involving the oscillation and the relaxation of the coalescing droplets. As the presence of a substrate can introduce extra resistance (Neogi & Miller 1982), different oscillation dynamics is expected compared with the coalescence of spherical droplets. Somwanshi *et al.* (2018) did experiments on the coalescence of two droplets attached to a hydrophobic surface in either pendent or sessile mode, and they found that the wall shear stress at the solid surface is much larger in the sessile mode than in the pendent mode. Jiang *et al.* (2019) studied the coalescence of two droplets with various wettability and found the capillary wave oscillation gets weaker with a decrease of the surface wettability. In a longer time scale, droplet dynamics is resisted by the viscous resistance from the bulk fluid

or from the contact line. This stage can take up to several seconds depending on the properties of the liquid and the substrate (Jiang *et al.* 2019). Some other phenomena can arise in this process, such as contact angle variations and contact line movements. For example, the experiments of droplet coalescence on partial wetting surfaces conducted by Narhe, Beysens & Nikolayev (2004) and Andrieu *et al.* (2002) showed that in the late stage, the droplet slowly relaxes to a circular shape which lasts six or seven orders of magnitude longer than that described by the bulk hydrodynamics. Such slow relaxation was demonstrated to be induced by the liquid–vapour phase change near the contact line. Zhang *et al.* (2015) observed complete stratification of the liquids of two droplets with different densities and viscosities followed by diffusive mixing in the composite droplet over a time scale of several minutes. For the coalescence of an impacting droplet with a sessile droplet, the induced surface jet can be either promoted or suppressed by the Marangoni flow, depending on the direction of the surface tension difference (Sykes *et al.* 2020*a*).

Most of the previous efforts on the coalescence of sessile droplets are restricted to miscible droplets (Borcia & Bestehorn 2013; Ahmadlouydarab & Feng 2014; Huang & Pan 2021). For the limited studies reporting directly or indirectly immiscible sessile droplet interaction, many focused on the equilibrium state after the interactions between the immiscible droplets, in which either they investigated the role of interfacial energy in forming a stable compound structure (Mahadevan, Adda-Bedia & Pomeau 2002) or they considered the effect of immiscible interface on a temporary equilibrium of a smaller oil droplet on a larger water droplet (Iqbal *et al.* 2017). Rostami & Auernhammer (2022) analysed the motion of the four-phase point (where the two liquids, the gas and the solid meet). From the perspective of a liquid spreading in a V-shape groove, they showed that the dynamics of this point is independent of contact line velocity but rather similar to the capillary flow in a tube. Another related work is by Xu *et al.* (2022), who experimentally and theoretically investigated the liquid bridge dynamics of a pendent immiscible droplet with a sessile droplet, and found that the immiscibility of the two liquids results in slower growth of the liquid bridge. These results illustrate the potential influence of miscibility and liquid wettability on immiscible droplet systems. However, when it comes to the coalescence of immiscible droplets on a substrate, the potential influences are expected to be much more complicated as they not only involve an extra immiscible interface (de Gennes, Brochard-Wyart & Quéré 2004), but also keep respective surface tensions and different interfacial tensions with the solid surface throughout the coalescence process. Thus, these different characteristics might have significant influences on the short-time dynamics of coalescing immiscible droplets, as well as on the subsequent long-time behaviours of the coalesced droplets. However, despite wide applications in multiphase processing (Xie *et al.* 2022), material synthesis (Winkelmann *et al.* 2013) and biological interaction of cells (Kusumaatmaja, May & Knorr 2021), a clear understanding of the coalescence of immiscible sessile droplets is still missing.

Based on an understanding of previous research on droplet coalescence, we experimentally investigate the coalescence dynamics of two immiscible droplets sitting on wettable surfaces. We identify three stages of coalescence, and analyse them in detail. We first study the fast growth of the liquid bridge after the coalescence and consider low-viscosity and high-viscosity oil droplets separately. We then analyse the oscillation dynamics of the coalescing droplets and identify the role of water–oil interfacial tension. Finally, the retraction of the coalesced droplet in a longer time scale is investigated, and the retraction dynamics for various immiscible droplet pairs with different surface tensions, interfacial tensions and viscosities is quantified.

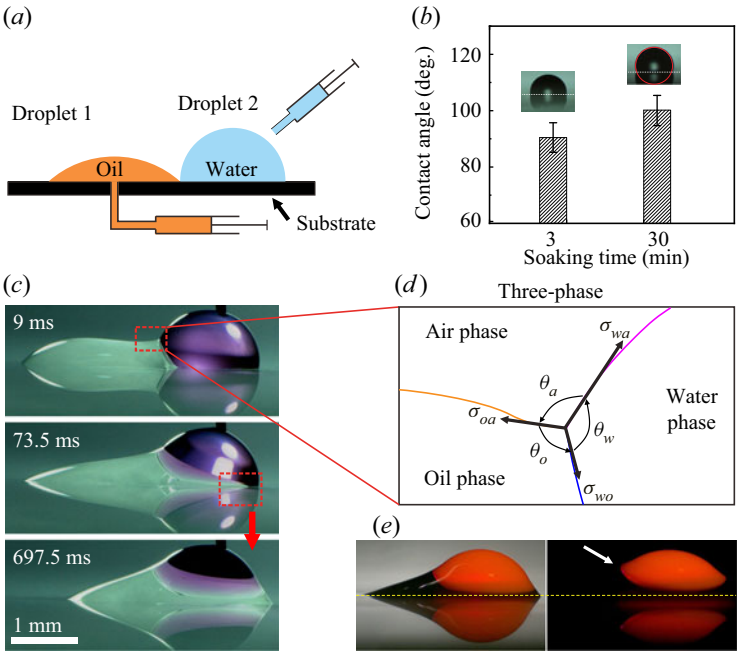

Figure 1. (*a*) Schematic diagram of the experimental set-up for the coalescence of two sessile immiscible droplets. (*b*) Contact angle of the substrates under two different soaking times in hydrophobic solution. (*c*) Typical snapshots during the coalescence of the two immiscible droplets. The water droplet was dyed red with Rhodamine B at a concentration lower than 0.1 wt%. (The needle embedded in the water droplet was used (here only) to deposit the water droplet on the substrate. The image used here is only to give a qualitative view of the four-phase capillary-driven flow in the contact region.) (*d*) Sketch of three liquid interfaces in the contact region, where the three-phase contact line generates three contact angles (θ_a, θ_w and θ_o). (*e*) Illustration of the dyed water droplet being displaced from the substrate by using different lighting methods: image to show the compound droplet with simultaneous front lighting and back lighting (left) and image to show the dyed water droplet alone with only front lighting (right). The dashed yellow line denotes the position of the substrate. The dyed water droplet is a mixture of 50 wt% glycerol solution with a low concentration of Congo red.

2. Experimental method

In the experiment, a water droplet with a known volume was first deposited on the substrate. Then, the coalescence was initiated by gradually introducing fluid into an oil droplet, whose size gradually increases until coalescence with the water droplet, as shown in figure 1(*a*). The introduction of the oil droplet was by pumping oil through a hole in the substrate (less than 0.1 mm in diameter), following methods similar to those of Karpitschka & Riegler (2010). The pre-deposited water droplet was placed at a certain distance from the hole to ensure approximately equal base radii of the two droplets. The typical size of the two droplets was kept around 1 mm or smaller to reduce the effect of gravity.

Droplet pairs of different liquids were used to vary the miscibility and wettability, as shown in table 1. The droplet with higher surface tension is the water phase and that with lower surface tension is the oil phase. For the water droplets, we used deionized water and its parameter is kept constant in our experiments. For the oil droplets, we used four kinds of liquids, namely silicone oil, alkane, high alcohol and brominated oil, which are all immiscible with water, but with different surface tensions and interfacial tensions. In addition, four sets of miscible droplet pairs were also prepared for comparison,

in which the oil droplets are produced by mixing different ratios of water with ethanol (shown in table 1). In some experiments, Rhodamine B was added to the water droplet to enhance the contrast between the two droplets, the concentration being lower than 0.1 wt%, which was tested to have negligible effects on the droplets' physical properties (Lu *et al.* 2020). Hydrophobic substrates were used in the experiment. The hydrophobic surface was made by soaking soda-lime glass in a hydrophobic solution (MesoPhobic-2000; MesoBioSystem) and then drying in an oven. Two kinds of substrates with different hydrophobicity were obtained by applying different soaking times, and the equilibrium water contact angle is $90 \pm 5^\circ$ for 3 min of soaking and $100 \pm 5^\circ$ for 30 min of soaking (as shown in figure 1*b*). For the first kind of hydrophobic substrates, the contact angles for the water–oil interface with the substrate measured from the water side are $137.4 \pm 2.1^\circ$ for silicone oils, $129.4 \pm 3.8^\circ$ for alkanes and $150.2 \pm 3.2^\circ$ for brominated oils. For the second kind of hydrophobic substrates, the contact angles for the water–oil interface with the substrate measured from the water side are $140.5 \pm 6.1^\circ$ for silicone oils, $136.0 \pm 4.5^\circ$ for alkanes and $157.8 \pm 2.1^\circ$ for brominated oils. The coalescence process was recorded using a high-speed camera (Phantom V1612) with a frame rate ranging from 10 000 to 250 000 frames per second. The typical frame exposure time is 3.38 μs, and the resolution is 256×128 for the highest frame rate. In addition, a microscopic lens (Navitar Zoom 6000) was used to achieve close-up views yielding a resolution of up to 6.37 μm pixel^{-1}. Backlight was applied by using a high-intensity fibre optic lamp along with a diffuser to illuminate the field of view to achieve uniform lighting. Moreover, in some experiments where the water droplet is dyed, the front lighting positioned to the side of the camera was supplemented to illuminate the droplet for clearer coloured visualization. To make sure we could capture the whole process, we started recording long before the contact of the two droplets. We then measure the bridge evolution by starting from the moment when we could first detect a discernible increase in the bridge height, which is a common practice in many studies of droplet coalescence processes (Eddi *et al.* 2013; Sprittles & Shikhmurzaev 2014). To further minimize the uncertainty, in our experiments, the initial height of the liquid bridge is limited to less than 5 % of the oil droplet height. For some cases with an unusually large initial bridge height (e.g. larger than 5 % of the oil droplet height, which may be due to the small spatial inaccuracies of the deposition of the second droplet), they were discarded. All the experiments were performed at room temperature and atmospheric pressure, where the room humidity was kept at over 30 % to avoid the electrostatic effect (Yokota & Okumura 2011).

3. Results and discussion

3.1. *Stages of the coalescence process*

We tracked the outer surface of the two coalescing immiscible droplets as well as their contact line, and the resulting image sequences are shown in figure 2 (also see supplementary movie 1 available at https://doi.org/10.1017/jfm.2023.685). During droplet coalescence, the governing forces involved are capillary force, inertia and viscous forces but could be dominant in different regions. The time scales which characterize different dynamics, therefore, could vary from around 1 to 2 ms to several minutes (Narhe *et al.* 2008). Based on the time scale and controlling forces (which are analysed in subsequent sections), we divided the coalescence process of two immiscible droplets into three primary stages, namely (I) the growth of the liquid bridge, (II) the oscillation of the coalescing sessile droplet and (III) the formation of a partially engulfed compound sessile

Liquid	Density ρ (kg m^{-3})	Dynamic viscosity μ (mPa s)	Surface tension σ (mN m^{-1})	Interfacial tension with water σ (mN m^{-1})
Water	1000	1.0	72	—
1-Octanol	812.4	7.4	27.5	8.4
1-Decanol	831.2	12.2	28.5	8.6
1-Undecanol	830	17.5	26.6	8.8
n-Dodecane	748.7	1.0	22.0	48.0
n-Hexadecane	770	3.9	22.1	44.4
Silicone oil (5 cSt)	913	4.6	18.7 ± 0.3	38.1 ± 0.4
Silicone oil (10 cSt)	930	9.3	18.7 ± 0.3	38.1 ± 0.5
Silicone oil (20 cSt)	950	18.9	19.8 ± 0.7	40.9 ± 0.5
Silicone oil (50 cSt)	960	48.0	20.4 ± 0.2	40.9 ± 0.5
Silicone oil (100 cSt)	960	96.0	20.1 ± 0.2	43.7 ± 0.4
Silicone oil (500 cSt)	970	465	20.0 ± 0.1	38.7 ± 0.2
Bromocyclopentane	1386	1.4 ± 0.05	33.2 ± 0.1	26
Bromocyclohexane	1336	2.2 ± 0.05	32.1 ± 0.1	26
EWM (1.000)	791.0	1.189	22.85	—
EWM (0.735)	832.9	1.950	24.49	—
EWM (0.552)	858.9	2.372	26.00	—
EWM (0.419)	884.4	2.791	27.45	—

Table 1. Physical properties of the liquids used in this study at 20 °C. The properties of the silicone oils are from Ji, Yang & Feng (2021), the alkanes from Goossens *et al.* (2011), the high alcohols from Yu *et al.* (2019) and the brominated oils from Rostami & Auernhammer (2022). EWM represents the ethanol–water mixture; values in parentheses represent the mole fraction of ethanol, and their properties are from Khattab *et al.* (2012).

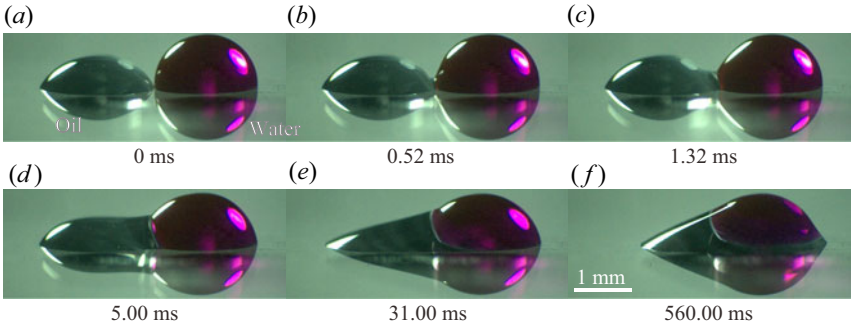

Figure 2. Typical time sequences of coalescence process of immiscible droplets. The two immiscible liquids are water and *n*-dodecane. The camera was tilted slightly downward (at an angle of 5° to the horizontal) to afford better observation. The volume ratio $V^* = V_o/V_w$ is 0.5117, where V_o and V_w are the volumes of the oil droplet and the water droplet, respectively. (A video clip for this process is available as supplementary movie 1.)

droplet (PECSD) and the subsequent retraction. Each stage is dominated by different forces and exhibits different phenomena.

(I) The growth of the liquid bridge. The instant of the first contact in the image sequence is defined as $t = 0$, as shown in figure 2(*a*). After the two droplets contact, a liquid bridge quickly builds up connecting the two droplets, as shown in figure 3(*a*). The large curvature formed on the liquid–vapour surface in the bridge area induces a large capillary force, which drives the quick growth of the liquid bridge. The growth rate decreases gradually as the bridge curvature reduces and as more liquid is set in motion. When the bridge height

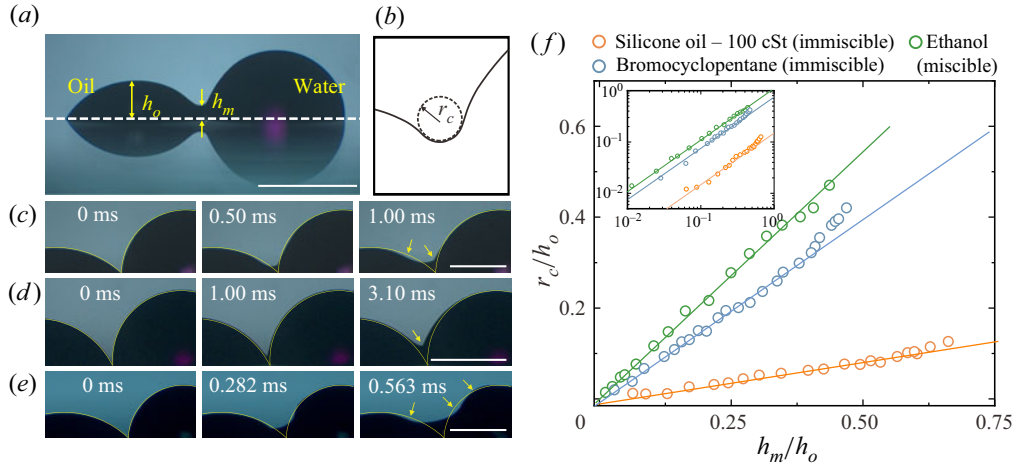

Figure 3. (*a*) The liquid bridge height $h_m(t)$ is defined as the vertical distance of the bridge neck to the substrate (white dashed line). (*b*) Illustration of the curvature radius (r_c) in the bridge region and is measured by fitting an inscribed circle to the surface shape in the bridge region following the method of Thoroddsen *et al.* (2007). (*c*) Snapshots showing the close-up of the liquid bridge of water droplet coalescence with a low-viscosity droplet (bromocyclopentane). The droplet volume ratio $V^* = 0.4315$. (*d*) Snapshots showing the close-up of the liquid bridge of water droplet coalescence with a high-viscosity droplet (silicone oil, 100 cSt). The droplet volume ratio $V^* = 0.635$. (*e*) Snapshots showing the close-up of the liquid bridge of water droplet coalescence with an ethanol droplet. The droplet volume ratio $V^* = 0.5894$. The overlaid yellow lines on the images are the initial shape of the two droplets. (*f*) Evolution of curvature radius (r_c) with bridge height. The inset shows the data in a log–log plot, where the solid lines have a slope of 1. Both the bridge height and the curvature radius are rescaled with the initial height of the oil droplet. The scale bars (white solid lines) are 1 mm. (Video clips for these processes are available as supplementary movies 2–4.)

is comparable with the height of the oil droplet (see figure 2*c*), the further growth of the liquid bridge is very slow, which can be seen from the time stamps below the snapshots. For example, it takes only around 1.32 ms for the bridge to grow to half of the oil droplet height, but it takes more than twice as long to reach the height of the initial oil droplet as shown in figures 2(*c*) and 2(*d*). When the bridge height increases to the oil droplet height, it indicates the finish of the first stage. Another prominent feature is the three-phase contact line on the surface of the droplets and as shown in figures 1(*c*) and 1(*d*), there is a net force along the water surface considering the relative magnitude of the three surface tensions and dynamic contact angles around the three-phase contact line. Consequently, one would expect a precursor film of oil to be driven onto the surface of the water (Cuttle *et al.* 2021; Sanjay *et al.* 2022) due to the surface tension gradient, which is often observed in three-phase flows. However, the precursor film is believed not to show up in this first stage since we can observe a sharp discontinuous interface in the bridge region as can be seen in figures 1(*c*) and 1(*d*). In addition, according to Koldeweij *et al.* (2019), the evolution of the leading edge of the oil film is $L(t) \sim \Delta\sigma^{1/2}t^{3/4}/(\mu\rho)^{1/4}$, where $\Delta\sigma$ is the surface tension difference and μ and ρ are the dynamic viscosity and density of the droplet of higher surface tension, respectively. Based on this relation, the time for the leading edge of an oil precursor film to reach the top of the water droplet is calculated to be as long as 3–4 ms, which exceeds the time scale of liquid bridge evolution (less than 2 ms in the present case). This further indicates that the precursor film would not influence the bridge growth.

In addition, during the growth of the liquid bridge, surface capillary waves, which are common in the coalescence of miscible droplets on solid surfaces (Eddi *et al.* 2013; Lee *et al.* 2013; Sykes *et al.* 2020*b*), are also observed in the present study for immiscible droplets (highlighted by the yellow arrows in figure 3*c*).

(II) The oscillation of the coalescing sessile droplet. Following the first stage, the coalescing droplet oscillates due to the surface tension and the inertia of the droplet. When the two droplets contact, their pressure difference can be estimated to be positive, $\Delta P = \sigma_{wa}/R_w - \sigma_{oa}/R_o > 0$, where R_w and R_o are the initial radii of the water and oil droplets, respectively. Therefore the water droplet first moves towards the oil droplet due to the relatively larger capillary pressure in the water droplet. After the accumulation of the inertia, the droplet overshoots even after the equilibrium point. Surface tension, then, causes the droplet to move backward. This process repeats as the interchange between the surface energy and the kinetic energy with some part of the energy being dissipated both in the bulk and in the contact line. The oscillation process is in a much longer time scale compared with the initial stage of liquid bridge growth.

(III) The formation of PECSD and its subsequent retraction. The third stage ensues as the droplet oscillation gradually relaxes. Driven by capillary forces and resisted by both inertia and viscous forces, the oil is seen surrounding the water droplet and filling under the water droplet. As a consequence, the water droplet can be displaced from the solid by the oil (see figures 2*e* and 1*e*), forming a PECSD on the solid surface. A clearer illustration of the displacement process can be seen in figure 1(*e*), which was obtained through different lighting methods. The PECSD then moves and contracts to decrease the contact area due to the minimization of the surface energy in a much longer time scale (see figure 2*f*). This slow stage is characterized by the four-phase capillary-driven flow and the retraction of the PECSD.

Since the three stages are controlled by different mechanisms, the dynamics of each stage is analysed in the subsequent sections.

3.2. *Growth of liquid bridge*

The dynamics of the first stage in the coalescence process is characterized by the rapid growth of the liquid bridge, as shown in figure 3(*a*). For two sessile droplets on a partial wetting surface, the coalescence of a water droplet with a high-viscosity oil droplet can be different from that with a low-viscosity oil droplet, because the liquid bridge growth could be affected by the extra viscous stress imposed by the substrate and the oil–water–air contact line that is unique to immiscible liquids. Therefore, the bridge growth is expected to exhibit different behaviours for oil droplets with low viscosity and high viscosity. Here, the high-viscosity droplet and low-viscosity droplet were differentiated by the Ohnesorge number $Oh = \mu_o/\sqrt{\rho_o h_o \sigma_{oa}}$, where h_o is the initial height of the oil droplet. Therefore, the low-viscosity oil droplet is identified to have Oh of $O(1)$ while the high-viscosity droplet is identified to have Oh much larger than 1.

We first focus on the coalescence of water droplets with low-viscosity oil droplets. For the coalescence of inviscid spherical droplets of identical liquids, the liquid bridge motion has been proved to be driven by capillary forces and resisted by inertia, and this short-time dynamics can be described as the inertia-controlled regime, where the bridge grows as $t^{1/2}$ (Duchemin *et al.* 2003). While the situation is markedly different in the case of sessile droplets, the evolution of the bridge height (h_m illustrated in figure 3*a*) is highly dependent on the droplet geometry before contact. The capillary pressure driving the bridge motion is scaled as $P_c \propto \sigma/w$, and the dynamic pressure in the fluids is estimated as $P_i \propto \rho(h_m/t)^2$,

where, for contact angles $\theta < 90^\circ$, the meniscus scale w was found to be proportional to the bridge height (Eddi *et al.* 2013): $w \propto h_m$. Then, based on the force balance analysis involving the capillary pressure and the dynamic pressure, the bridge growth is predicted to follow $h_m \propto t^{2/3}$ (Eddi *et al.* 2013).

In this study of immiscible droplet coalescence, we can see from figure 3(*c–e*) that the bridge region mainly appears on the lower-surface-tension droplet (i.e. oil), and the bridge height exhibits an almost consistent power-law growth $h_m \propto t^{\alpha}$ as shown in figure 4(*a*). By referring to the fitting method adopted by Dekker *et al.* (2022), the exponent was obtained by conducting linear fitting in a log–log plot (to determine the first contact instant accurately, the time was slightly shifted until the fitting can achieve the smallest residual sum of squares). We can see that the exponents are all distributed around 2/3 (see figure 4*b*). The rapid bridge growth is driven by the large capillary pressure in the bridge region induced by the large curvature. We then trace the radius of curvature during the bridge growth as shown in figure 3(*f*), and we can see that the curvature follows approximately a linear growth with the bridge height for both the miscible droplet pairs and immiscible droplet pairs. This linear relationship indicates that the immiscible interface does not change the evolving geometrical relationship between the bridge curvature and the bridge height. When incorporating ($r_c \propto h_m$) into the balance between capillary pressure $P_c \propto \sigma/w$ and dynamic pressure $P_i \propto \rho(h_m/t)^2$, it gives the same 2/3 power law of bridge growth of immiscible droplets. However, when comparing the time that it takes for the liquid bridge height to reach half of the initial height of the oil droplet (see figure 4*f*), the time for immiscible droplets could be two to three times longer than that for miscible droplets of similar low viscosity. The comparatively longer bridge growth time of immiscible droplets indicates that the growth speed is lower. This lower growth speed can be attributed to the lower kinetic energy converted from the released surface tension energy during the coalescence, as an extra immiscible interface is formed in the immiscible droplets. This immiscible interface would consume part of the released energy that should be converted to kinetic energy. In contrast, this water–oil interface is absent in miscible droplet coalescence.

These results show that for two droplets of approximately inviscid fluids, the immiscibility of the two droplets has no significant effect on the growth scaling of the liquid bridge height, which follows the same power law as that of the inertial coalescence of the same droplets, i.e. $h_m \propto t^{2/3}$, but it can substantially decrease the growth speed of liquid bridges. This is mainly because the curvature of the bridge is mostly on the lower-surface-tension droplet. Therefore, the large capillary force driving the bridge growth is provided by the oil droplet. Though a water–oil interface is formed after the contact of the two droplets, its size is small and it has a certain distance to the position of the minimum bridge height. Hence, the effect of the water–oil interface on the bridge growth is weak. Therefore, the growth of the liquid bridge height follows the $h_m \propto t^{2/3}$ power law.

Further, it is noted that, in the present configuration, the two droplets have different contact angles and, therefore, different sizes. To look into the possible size effect, we first, by assuming the length scale that influences the bridge growth to be the initial oil droplet height h_o, construct a characteristic time scale $t_\sigma = \sqrt{\rho_{avg} {h_o}^3/\Delta\sigma}$, where $\rho_{avg} = (\rho_o + \rho_w)/2$ is the average density and $\Delta\sigma = \sigma_{wa} + \sigma_{oa} - \sigma_{wo}$ is based on the net interfacial tension as shown in figure 1(*d*). The bridge growth data in figure 4(*a*) can then be collapsed together (see figure 5*b*), which indicates that the bridge growth is predominantly influenced by the size of the oil droplet compared with the water droplet.

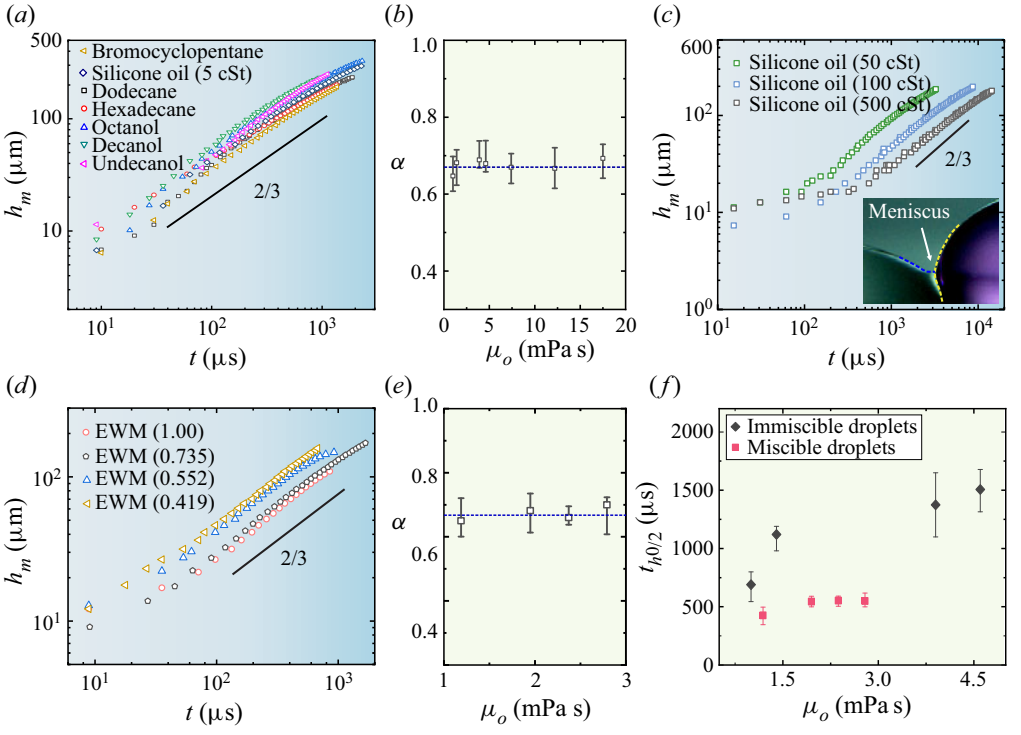

Figure 4. (*a*) Evolution of the liquid bridge height for water droplets with different low-viscosity oil droplets. The inset shows the data in a linear plot. (*b*) Fitted exponent α under various oil droplets with different viscosities; the dashed line shows $\alpha = 2/3$. (*c*) Evolution of the liquid bridge height for water droplets with different high-viscosity oil droplets. The inset shows the oil meniscus between the oil droplet and the water droplet. (*d*) Evolution of the liquid bridge height for water droplets with different miscible droplets made of EWM. (*e*) Fitted exponent α of the coalescence of miscible droplets with different viscosities. The dashed line shows $\alpha = 2/3$. (*f*) Time that it takes for the liquid bridge to reach half of the initial height of the oil droplet.

It also indicates that the properties of the oil droplets affect the time scale of the bridge growth but do not alter the 2/3 scaling. Similarly, in the experiments of coalescence of asymmetric miscible droplets (Pawar *et al.* 2019*a*), where the contact angle of one droplet is smaller than 90° and is 90° for the other, the bridge growth is found to be dominated by the droplet of contact angle smaller than 90° and to follow the same 2/3 power law but with different prefactors. Here, we do not intend to go further into discussing the exact prefactors but aim to test the power-law dynamics of the bridge growth. In our experiments, the contact radii of the two droplets are limited to be approximately the same to minimize the possible relative size effect.

Moreover, for the coalescence of water droplets with high-viscosity oil droplets (e.g. silicone oils of viscosities ranging from 50 to 500 cSt), the bridge growth is different from that of the low-viscosity droplets in many ways. First, no distinct surface wave is observed on the surface of droplets, while a much sharper curvature in the bridge region is observed, similar to the droplet coalescence scenario of two high-viscosity miscible droplets (Thoroddsen *et al.* 2007). However, seen from the log–log plot in figure 3(*f*), the curvature radius also evolves nearly linearly within a period, which may account for the 2/3 power-law growth of the bridge. Second, the high viscosity influences the initial growth of the liquid bridge, which leads to a much slower process, as shown in

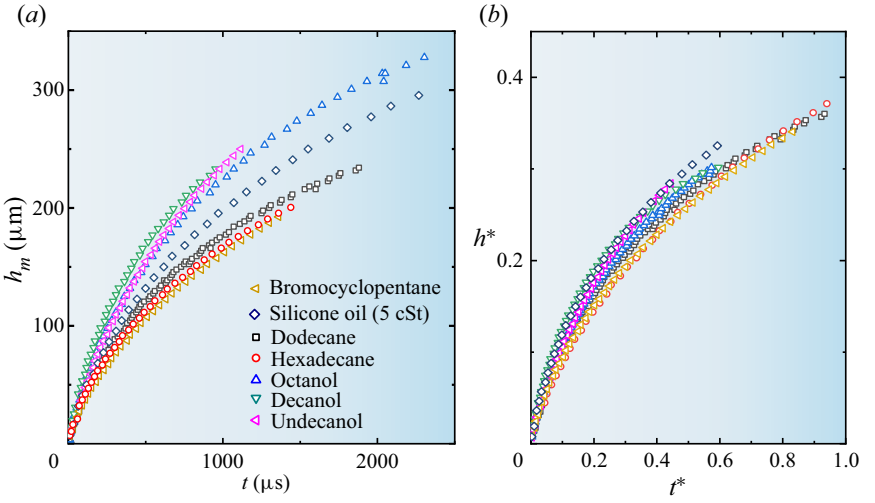

Figure 5. (*a*) Linear plot of the data in figure 4(*a*). (*b*) Rescaling of the data, where the bridge height was scaled by the initial oil droplet height $h^* = h_m/h_o$, and the time was rescaled with the constructed time scale $t^* = t/t_\sigma$.

the log–log plot of the data (when $t \ll 1000$ μs in figure 4*c*). We speculate that this slow motion could be correlated with the extra viscous resistance in the meniscus (see the inset of figure 4*c*), which forms when the oil droplet contacts the water droplet. The sharp curvature of the meniscus also indicates large stress in that region, which is reminiscent of the case of a water droplet slowly moving on a viscous-oil-impregnated surface (Keiser *et al.* 2017): during the moving process, the oil meniscus with a sharp curvature was also found surrounding the water droplets and was proposed to be responsible for significant viscous resistance.

3.3. *Oscillation of the coalescing droplet*

Due to the liquid velocities induced by the bridge growth and the released surface energy resulting from the coalescence, the droplet surface undergoes further deformation, and then the droplet bulk fluid oscillates. Since the two droplets have different surface tensions and different contact angles, the imbalanced Laplace pressure further generates an obvious horizontal movement. Therefore, we trace the horizontal movement of the droplet centroid, ΔX, in the side-view images by image processing, which could represent the bulk movement of the droplet (Somwanshi, Muralidhar & Khandekar 2017; Zhao *et al.* 2021), to investigate the droplet oscillation dynamics. In the present sessile droplet configuration, the values of Bond number $Bo = \rho g R^2/\sigma$ are rather low, being around 0.034 and 0.078 for 1 mm water droplet and oil droplet in air, respectively. According to the analysis of droplet oscillation in Lamb (1924), considering the contribution of both surface tension and gravity, the oscillation frequency follows $f = \sqrt{g(2l+1)/[2l(l-1)R] + \sigma l(l-1)(l+2)/(\rho R^3)}/2\pi$, where l is the oscillation degree mode ($l \geqslant 2$). The effect of gravity on the oscillation frequency is estimated to be less than 1 % in our experiments. This indicates that gravitational forces are less predominant than capillary forces for small droplets, and that capillary forces serve as the dominant restoring force in the present study of the oscillation process.

The oscillation for different immiscible droplet pairs shows different behaviours, as shown in figure 6(*a–c*). For example, in the case of a silicone oil droplet with a water droplet, the oscillation shows a much larger initial displacement amplitude and a lower oscillation period than that when the oil droplet is *n*-octanol or *n*-decanol. This different oscillation behaviour should not be attributed to the viscous effect in the low-viscosity liquid, because the viscosity of the 10 cSt silicone oil droplet (9.3 mPa s, in figure 6*a*) is even higher than that of the octanol droplet (7.4 mPa s, shown in figure 6*b*). Of course, when the oil droplet has a high viscosity, no oscillation behaviour is observed as shown in figure 6(*c*), which can be explained by the damping effect caused by the high viscosity (Khismatullin & Nadim 2001). However, for the cases shown in figures 6(*a*) and 6(*b*), the fluid viscosities are always low (3.9–12.2 mPa s). Considering surface tension is the main cause for the oscillation in droplet coalescence dynamics where it is free of external forces (Chashechkin 2019), and the liquids used in figures 6(*a*) and 6(*b*) have rather different oil–water interfacial tensions and also different surface tensions, we thus speculate that both the interfacial tension and the surface tension should have a marked influence on the droplet oscillation dynamics, and the influence of interfacial tension on the droplet oscillation dynamics should be further investigated. To avoid the damping effect of high viscosity, low-viscosity oil droplets are then used to analyse the oscillation behaviour.

We first consider the oscillation process from the perspective of energy conservation. The immiscible water–oil interface would contain a non-negligible portion of the released surface energy which is proportional to the interfacial tension σ_{wo}, resulting in a decreased energy to be converted to the droplets' kinetic energy given that the viscous dissipation influence is comparably smaller for the low-viscosity droplets used. Therefore, the droplet pair with a larger water–oil interfacial tension would end up in a smaller displacement amplitude, as shown in figure 6(*a*). Further, by plotting the oscillation periods under different interfacial tensions (see figure 7*a*), we can see that the oscillation periods show a generally decreasing trend with the interfacial tension. This variation indicates that the interfacial tension, which is unique to the immiscible system, could markedly affect the coalescence process and lead to different oscillation dynamics. Secondly, the surface tension can quantify an oscillating droplet's ability to restore (Deepu, Chowdhuri & Basu 2014), and therefore could also affect the oscillation periods. However, here, both the oil surface tensions and the water–oil interfacial tensions are different, indicating that their frequency differences cannot be attributed to the surface tension or interfacial tension alone. For example, the oscillation period of the water–octanol droplet pair is almost twice as long as that of the water–*n*-hexadecane droplet pair (these two droplet pairs have different surface tensions and interfacial tensions) as shown in figures 6(*a*) and 6(*b*). Therefore, both the surface tension and the interfacial tension should be considered in the analysis of the oscillation dynamics of the coalescing droplets.

Though the role of surface tension in the oscillation of simple droplets has been widely studied (Khismatullin & Nadim 2001; Menchaca-Rocha *et al.* 2001; Chireux *et al.* 2015; Yuan *et al.* 2015; Zhao *et al.* 2021), the oscillation of a coalescing droplet, which is produced after the coalescence of two immiscible droplets, is more complex. Here, we investigate the oscillation dynamics by considering both surface tensions and water–oil interfacial tensions. The mass–spring system is commonly used to model the long-time oscillation behaviour of coalescing droplets, during which surface tension is the restoring force opposing the deformation, and the oscillation of the coalescing droplet can be considered as a capillary–inertia system (Chireux *et al.* 2015; Yuan *et al.* 2015). An immiscible liquid system in capillary–inertia controlled processes (such as droplet impact and oscillation) can be regarded as a parallel spring system (Bernard *et al.* 2020), and

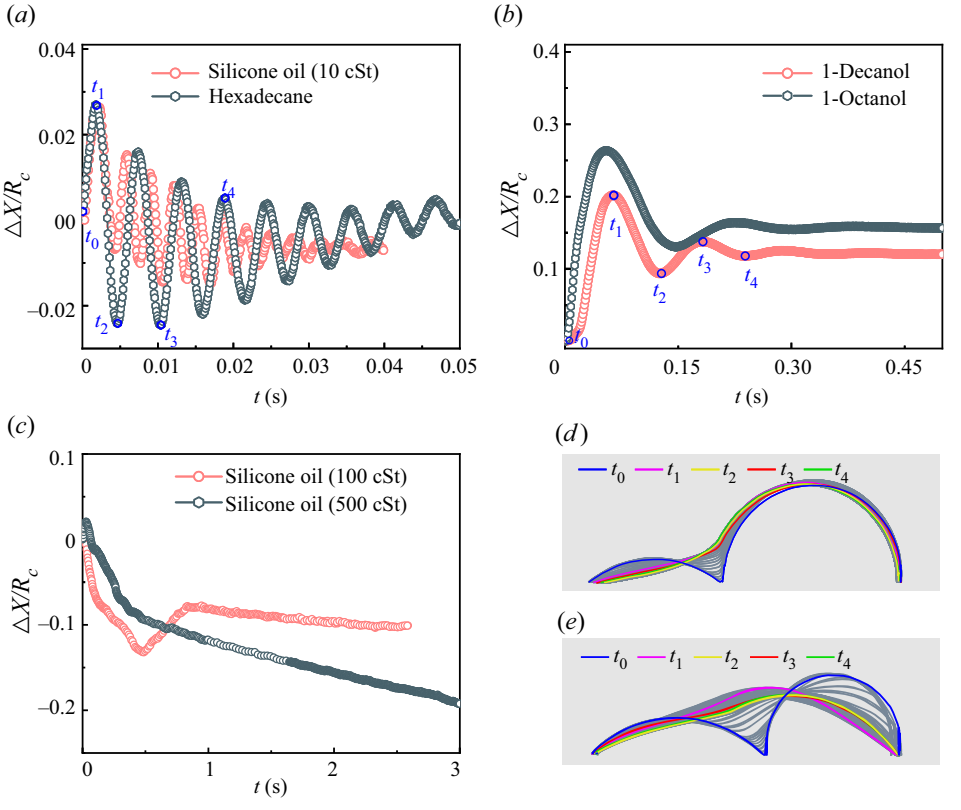

Figure 6. Temporal evolution of the normalized horizontal centroid displacement after the coalescence of a water droplet with different oil droplets: (*a*) silicone oil (10 cSt) and hexadecane; (*b*) *n*-decanol and *n*-octanal; (*c*) silicone oil (100 and 500 cSt). Radius R_c is the equivalent radius of the two droplets, $R_c = \sqrt[3]{3(V_o + V_w)/(4\pi)}$, and V_o and V_w represent the volumes of water droplets and oil droplets, respectively. Evolution of the outline of the coalescing droplet: (*d*) water droplet with hexadecane droplet; (*e*) water droplet with *n*-decanol droplet. The corresponding moments are marked in (*a*,*b*).

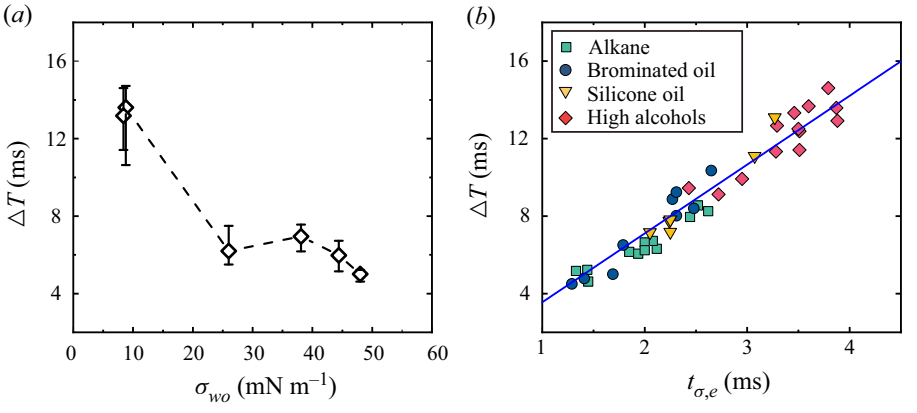

Figure 7. (*a*) Oscillation period ΔT of the coalescing immiscible droplets versus the water–oil interfacial tension. (*b*) Oscillation period ΔT versus the capillary time scale $t_{\sigma,e}$ in (3.1).

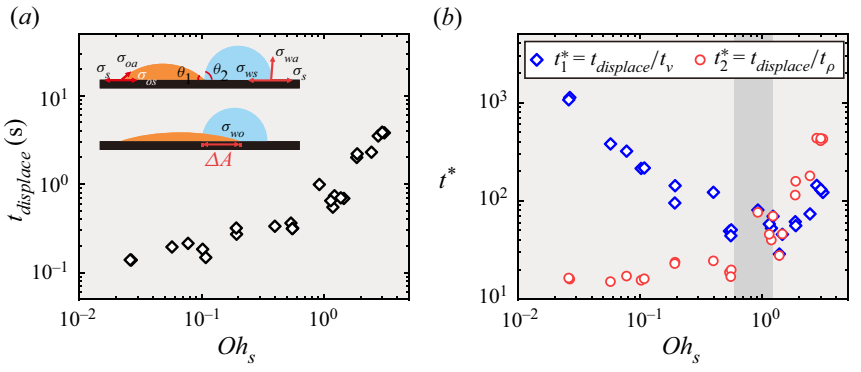

Figure 8. (*a*) Time taken for the oil droplet to displace the water droplet from the solid substrate $t_{displace}$ under different Oh_s. The inset illustrates the interface shapes before and after the displacement process, where σ_s, σ_{ws} and σ_{os} are the interfacial tensions of solid–air, water–solid and oil–solid, respectively, and σ_{oa}, σ_{wa} and σ_{wo} are the interfacial tensions of oil–air, water–air and water–oil, respectively. (*b*) Displacement time $t_{displace}$ scaled with an inertia time scale t_ρ (red circles) and a viscous time scale t_v (blue diamonds).

the equivalent spring constant can be represented by the summation of surface tensions and water–oil interfacial tension. With such an analogy, we can first obtain an equivalent spring constant, which is $\sigma_e = \sigma_{wa} + \sigma_{oa} + \sigma_{wo}$.

Next, in order to see how the oscillation dynamics is related to the interfacial tension, we evaluate the capillary time scale by taking the equivalent spring constant (i.e. the effective capillary force) into consideration:

$$t_{\sigma,e} = \sqrt{\frac{m_w + m_o}{\sigma_e}} = \sqrt{\frac{\pi[\rho_w(3{r_w}^2 h_w - {h_w}^3) + \rho_o(3{r_o}^2 h_o - {h_o}^3)]}{6\sigma_e}}, \tag{3.1}$$

where r_w, h_w and r_o, h_o are the initial contact radii and heights of the water and oil droplets, respectively. We then plot the oscillation period versus this proposed capillary time scale $t_{\sigma,e}$. As shown in figure 7(*b*), the oscillation period ΔT exhibits a good linear relationship with the proposed capillary time scale $t_{\sigma,e}$, i.e. $\Delta T \propto t_{\sigma,e}$. The linear relationship indicates that $t_{\sigma,e}$ properly captures the two immiscible droplets' oscillation dynamics. It also confirms that apart from the surface tensions of the two liquids, the interfacial tension between the two liquids also acts as a non-negligible restoring force which affects the oscillation.

3.4. *Formation and retraction of PECSD*

After the contact of the two immiscible droplets, in a much longer time scale, the oil is seen spreading below the water droplet driven by the unbalanced capillary force at the liquid–solid interface. Such a capillary-driven flow will eventually lead to the water droplet being displaced by the oil on the substrate, as illustrated in the inset of figure 8(*a*), which then forms the PECSD. This PECSD then contracts to further lower the system energy.

We analyse the droplet displacing process by referring to the capillary-driven flow in the three-phase system, whose dynamics is characterized by the spreading parameter $S = \sigma_{ij} - (\sigma_{ik} + \sigma_{jk})$ (Adamson & Gast 1967). It should be noted that for our four-phase flow (i.e. water, oil, air and solid), the interfacial tension between the liquid and the solid also influences the spreading dynamics of the droplet (Bonn *et al.* 2009), indicating that the wettability of the solid surface should be taken into consideration. We consider this

capillary-driven flow from the energetic perspective. When an area ΔA on the substrate is displaced by the oil (as illustrated in figure 8a), the released surface energy can be written as

$$\Delta E_\sigma = \Delta A(\sigma_{oa} + \sigma_{ws}) - \Delta A(\sigma_{wo} + \sigma_{os}), \tag{3.2}$$

where ΔA is the surface area where the water–solid contact area is replaced by the oil–water and oil–solid surfaces. It should be noted that this is a simplified form, as there is a difference between the area along the substrate ΔA and the area along the curved surface of the droplet ΔA_2. The two areas can be correlated with a geometrical relation: $\Delta A_2 = \Delta A/\cos\alpha$, where α is the contact angle of oil below the water droplet. Since α is measured to be small (around 15°), $\cos\alpha$ is close to one. Their respective surface tensions are illustrated in the inset of figure 8(a). The oil–solid and the water–solid interfacial tensions can be obtained from the Young equation, which relates the equilibrium contact angle of a sessile droplet with three surface tensions. For the oil droplet, the oil–solid interfacial tension can be determined as

$$\sigma_{os} = \sigma_s - \sigma_{oa}\cos\theta_1. \tag{3.3}$$

For the water droplet, the water–solid interfacial tension can be determined as

$$\sigma_{ws} = \sigma_s - \sigma_{wa}\cos\theta_2. \tag{3.4}$$

Substituting (3.3) and (3.4) into (3.2), ΔE_σ is obtained as

$$\Delta E_\sigma = \Delta A\left[\sigma_{oa}(1 + \cos\theta_1) - \sigma_{wo} - \sigma_{wa}\cos\theta_2\right]. \tag{3.5}$$

The capillary-driven flow is favoured when the released surface energy $\Delta E_\sigma > 0$. Inspired by the spreading parameter S which characterizes the wetting state of a three-phase system, we here define $S_\sigma = \sigma_{oa}(1 + \cos\theta_1) - \sigma_{wo} - \sigma_{wa}\cos\theta_2$ as the spreading parameter in the present system. In this case, the displacement of water droplets happens under a positive S_σ, which otherwise would not happen if S_σ is negative. We further test this spreading parameter S_σ by applying it to the experiments of Rostami & Auernhammer (2022), where the merging of two immiscible droplets on solid surfaces was studied. In their experiments, the position of the water droplet was found to show no changes and S_σ was calculated to be negative. We, therefore, use S_σ to quantify the driving force of this four-phase capillary-driven flow.

We then trace the time taken for the oil droplet to displace the water droplet from the solid surface, $t_{displace}$, which is identified from the moment when the two droplets make contact to the moment when the oil reaches the opposite end of the water droplet. During this process, both inertia and viscous forces could resist the flow. The relative importance of these forces can be measured using a modified Ohnesorge number based on the spreading parameter S_σ:

$$Oh_s = \frac{\mu_o}{\sqrt{\rho_{avg} R_c S_\sigma}}, \tag{3.6}$$

where R_c is the equivalent radius of the two droplets: $R_c = \sqrt[3]{3(V_o + V_w)/(4\pi)}$.

The variation of the displacement time against Oh_s is shown in figure 8(a). For a small Oh_s, the displacement time does not show significant variation. In contrast, when $Oh_s > 1$, the displacement time is much longer and shows significant variations. Further, based on the spreading parameter S_σ, two relevant time scales can be involved for the flow from dimensional analysis: a viscous time scale $t_v = \mu_o R_c/S_\sigma$ and an inertia time scale $t_\rho = \sqrt{(m_w + m_o)/S_\sigma}$. Here, in the inertia time scale, we choose the total mass of the oil droplet

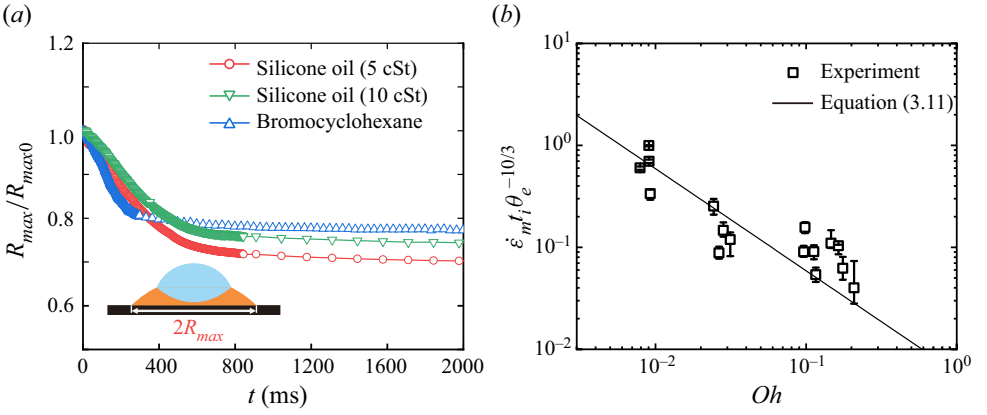

Figure 9. (*a*) Evolution of the normalized contact radius for three different liquid pairs. The inset illustrates the maximum contact radius R_{max} of PECSD during retraction. Radius R_{max0} is the maximum contact radius of PECSD at the outset of retraction. (*b*) Variation of $\dot{\varepsilon}_m t_i \theta_e^{-10/3}$ as a function of Oh. The solid line denotes the relationship given in (3.11) with L being of the same order as the droplet size, ∼1 mm, and λ being of the order of nanometre scale, ∼1 nm (de Gennes 1985; Bonn *et al.* 2009).

and the water droplet ($m_w + m_o$) to be the characteristic mass, considering that the inertia of both droplets could resist the flow. The measured displacement time is first rescaled with the inertia time scale t_ρ, as shown in figure 8(*b*). The rescaled results show that it is almost a constant for $Oh_s < 1$, but increases with Oh_s when $Oh_s > 1$. In contrast, by rescaling the data with the viscous time scale t_ν, different behaviour can be observed: the dimensionless displacement time shows a significant decrease with Oh_s when $Oh_s < 1$, and increases when $Oh_s > 1$. The shaded area in figure 8(*b*), in which Oh_s is around 1, indicates a transitional regime where the viscous and inertia contributions are comparable. The rescaled result illustrates that for low-viscosity fluids, the droplets' inertia is the main resistance in this capillary-driven flow, while with the increase of Oh_s, both the inertia and viscous forces would have a non-negligible resistance to this four-phase capillary-driven flow.

As the oil displaces the water droplet on the solid surface, a PECSD is formed and is observed to retract at a much slower time scale to further lower the system's energy. Such retraction motion is relatively fast at the beginning of the retraction, and then the retraction speed gradually decreases, as is shown in figure 9(*a*). Similar retraction processes are common to see in spreading droplets (Andrieu *et al.* 2002; Siahcheshm, Goharpey & Foudazi 2018). A measure of the droplet retraction is the relative retraction rate, defined as $\dot{\varepsilon} = \dot{R}(t)/R(t)$, where $R(t)$ is the contact radius of the compound droplet and the overdot indicates the derivative with respect to time. The retraction rate is a critical parameter in characterizing the retraction of sessile droplets (Siahcheshm *et al.* 2018).

We then investigate the retraction motion from the energy balance. First, by using the parameters of this PECSD defined before along with the maximum retraction velocity u_m, we can have a quick estimation of the Weber number, $We = \rho_{avg} R_c u_m^2/\sigma_e$, which is of $O(10^{-5})$. In this case, due to the low Weber number of this retraction process, the inertia can be safely neglected and the rate of work done by capillary forces can be assumed to be equal to the rate of viscous dissipation (Bonn *et al.* 2009). Further, with a low capillary number, the viscous dissipation is concentrated in the region close to the contact line (de Gennes 1985). By considering the flow near the contact line of the retracting droplet, the

rate of viscous dissipation in the receding corner per unit length of the contact line is expressed as (de Gennes *et al.* 2004)

$$\Phi_d = \frac{3\mu_o U^2}{\theta_r}\int_0^\infty \frac{\mathrm{d}x}{x}, \tag{3.7}$$

where $U = \dot{R}(t)$ is the retraction velocity. Since the retraction mainly happens in the direction of the major axis, $R(t)$ is defined to be the time-dependent contact radius of the compound droplet measured in the direction of the major axis. According to the de Gennes approximation, $\int_0^\infty \mathrm{d}x/x \approx \int_\lambda^L \mathrm{d}x/x = \ln(L/\lambda)$, where the macroscopic and microscopic cut-off lengths L and λ are calculated as the droplet size and the molecular size, respectively (de Gennes 1985).

The work done by the capillary force per unit length of the contact line can be then expressed as

$$\Phi_f = \sigma_{oa}[\cos\theta_r(t) - \cos\theta_{r,e}]U, \tag{3.8}$$

where $\theta_r(t)$ is the dynamic receding contact angle and $\theta_{r,e}$ is the equilibrium receding contact angle and can be simplified as the equilibrium contact angle. Such simplification is valid in this slow process as the capillary number $Ca = \mu_o U/\sigma_{oa}$ is estimated to be of $O(10^{-4})$, being much smaller than 1 (Edwards *et al.* 2016). Further, in the limit of $\theta_r < \theta_e \ll 1$, a first-order approximation of the Taylor expansion is used, $\cos\theta_r(t) \approx 1 - \theta_r^2/2$, $\cos\theta_e(t) \approx 1 - \theta_e^2/2$, and then (3.8) can be rewritten as $\Phi_f = \sigma_{oa}[\theta_e^2 - \theta_r^2(t)]U/2$. The balance between Φ_f and Φ_d then gives

$$\frac{\dot{R}(t)}{R(t)} = \frac{\sigma_{oa}}{6\mu_o \ln L/\lambda}\left(\frac{\pi}{3V_t}\right)^{1/3}[\theta_e^2 - \theta_r^2(t)]\theta_r^{4/3}(t), \tag{3.9}$$

where V_t is the total volume of the coalescing droplet, which can be estimated by approximating it as a spherical cap, i.e. $V_t = \pi\theta_r(t)R^3(t)/4$. Then, we can obtain the maximum retraction rate by finding $\mathrm{d}[\dot{R}(t)/R(t)]/\mathrm{d}t = 0$:

$$\dot{\varepsilon}_m = \max\left[\frac{\dot{R}(t)}{R(t)}\right] = \frac{\sigma_{oa}}{10\mu_o \ln(L/\lambda)}\left(\frac{\pi}{3V_t}\right)^{1/3}\left(\frac{2}{5}\right)^{2/3}{\theta_e}^{10/3}. \tag{3.10}$$

By rearranging (3.10), a relationship for the maximum retraction rate can be obtained:

$$\dot{\varepsilon}_m t_i {\theta_e}^{-10/3} = \frac{1}{10\ln(L/\lambda)}\left(\frac{1}{25}\right)^{1/3} Oh^{-1}, \tag{3.11}$$

where $t_i = \sqrt{\rho_{avg}R_c^3/\sigma_{oa}}$ is an inertia–capillary time scale and $Oh = \mu_o/\sqrt{\rho_{avg}R_c\sigma_{oa}}$ is a modified Ohnesorge number for the retraction process.

Comparing this theoretical model in (3.11) with the experimental data, we can see a good agreement as shown in figure 9(*b*), confirming the above-proposed mechanism that the retraction of the PECSD is dominated by the viscous dissipation occurring in the receding wedge of the contact line.

4. Conclusions

In this article, we have investigated the coalescence of two sessile droplets of immiscible fluids on a partial wetting surface. The coalescence process is divided into three stages,

namely (I) the growth of the liquid bridge, (II) the oscillation of the coalescing sessile droplet and (III) the formation of a PECSD and the subsequent retraction. Stage I characterizes the rapid growth of the liquid bridge. For low-viscosity oil droplets, the bridge dynamics follows a power-law growth similar to that of miscible droplets. When the oil droplet viscosity increases, we observe a much slower bridge growth in the early time of the first stage, which could be attributed to the extra viscous resistance in the meniscus formed near the oil–water–air contact line. In stage II, the coalescing sessile droplet oscillates. For high-viscosity oil droplets, the oscillation could be quickly damped out, while for low-viscosity droplets, the oscillation is controlled by inertia and capillary forces. By defining a modified capillary time scale, we show that the interfacial tension between the two immiscible liquids functions as a non-negligible resistance to the oscillation. In stage III, a PECSD first forms and then retracts. The formation of the PECSD is characterized by the displacement of water by the oil droplet, and could be resisted by viscous forces or inertia depending on a modified Ohnesorge number Oh_s, which incorporates the influence of the solid surface wettability. To quantify the retraction rate, a model is proposed based on the energy balance, and it demonstrates that the viscous resistance concentrated in a region close to the contact line dominates the slow retraction process.

We expect that the results and insights derived here could be helpful to applications involving microdroplet manipulation, droplet-based biochemical reactions and liquid removal. To realize better control of droplets in practical applications, external forces can also be adopted, such as magnetic fields (Li *et al.* 2020; Shyam, Dhapola & Mondal 2022) and electric fields (Anand *et al.* 2019), which require further study in this area.

Supplementary movies. Supplementary movies are available at https://doi.org/10.1017/jfm.2023.685.

Funding. This work was supported by the National Natural Science Foundation of China (grant nos. 52176083 and 51921004).

Declaration of interests. The authors report no conflict of interest.

Author ORCIDs.
Zhizhao Che https://orcid.org/0000-0002-0682-0603.

References

Aarts, D.G.A.L., Lekkerkerker, H.N.W., Guo, H., Wegdam, G.H. & Bonn, D. 2005 Hydrodynamics of droplet coalescence. *Phys. Rev. Lett.* **95** (16), 164503.

Adamson, A.W. & Gast, A.P. 1967 *Physical Chemistry of Surfaces*, vol. 150. Interscience.

Ahmadlouydarab, M. & Feng, J.J. 2014 Motion and coalescence of sessile drops driven by substrate wetting gradient and external flow. *J. Fluid Mech.* **746**, 214–235.

Anand, V., Roy, S., Naik, V.M., Juvekar, V.A. & Thaokar, R.M. 2019 Electrocoalescence of a pair of conducting drops in an insulating oil. *J. Fluid Mech.* **859**, 839–850.

Andrieu, C., Beysens, D.A., Nikolayev, V.S. & Pomeau, Y. 2002 Coalescence of sessile drops. *J. Fluid Mech.* **453**, 427–438.

Bernard, R., Baumgartner, D., Brenn, G., Planchette, C., Weigand, B. & Lamanna, G. 2020 Miscibility and wettability: how interfacial tension influences droplet impact onto thin wall films. *J. Fluid Mech.* **908**, A36.

Beysens, D.A. & Narhe, R.D. 2006 Contact line dynamics in the late-stage coalescence of diethylene glycol drops. *J. Phys. Chem.* B **110** (44), 22133–22135.

Bonn, D., Eggers, J., Indekeu, J., Meunier, J. & Rolley, E. 2009 Wetting and spreading. *Rev. Mod. Phys.* **81** (2), 739–805.

Borcia, R. & Bestehorn, M. 2013 Partial coalescence of sessile drops with different miscible liquids. *Langmuir* **29** (14), 4426–4429.

CHA, H., XU, C., SOTELO, J., CHUN, J.M., YOKOYAMA, Y., ENRIGHT, R. & MILJKOVIC, N. 2016 Coalescence-induced nanodroplet jumping. *Phys. Rev. Fluids* **1**, 064102.

CHASHECHKIN, Y.D. 2019 Oscillations and short waves on a free falling drop surface (experiment and theory). In *Conference Topical Problems of Fluid Mechanics 2019: Proceedings* (ed. D. Šimurda & T. Bodnár), pp. 45–52.

CHIREUX, V., FABRE, D., RISSO, F. & TORDJEMAN, P. 2015 Oscillations of a liquid bridge resulting from the coalescence of two droplets. *Phys. Fluids* **27** (6), 062103.

CHOI, K., NG, A.H.C., FOBEL, R. & WHEELER, A.R. 2012 Digital microfluidics. *Annu. Rev. Anal. Chem.* **5** (1), 413–440.

CUTTLE, C., THOMPSON, A.B., PIHLER-PUZOVIĆ, D. & JUEL, A. 2021 The engulfment of aqueous droplets on perfectly wetting oil layers. *J. Fluid Mech.* **915**, A66.

DEEPU, P., CHOWDHURI, S. & BASU, S. 2014 Oscillation dynamics of sessile droplets subjected to substrate vibration. *Chem. Engng Sci.* **118**, 9–19.

DEKKER, P.J., HACK, M.A., TEWES, W., DATT, C., BOUILLANT, A. & SNOEIJER, J.H. 2022 When elasticity affects drop coalescence. *Phys. Rev. Lett.* **128** (2), 028004.

DUCHEMIN, L., EGGERS, J. & JOSSERAND, C. 2003 Inviscid coalescence of drops. *J. Fluid Mech.* **487**, 167–178.

EDDI, A., WINKELS, K.G. & SNOEIJER, J.H. 2013 Influence of droplet geometry on the coalescence of low viscosity drops. *Phys. Rev. Lett.* **111** (14), 144502.

EDWARDS, A.M.J., LEDESMA-AGUILAR, R., NEWTON, M.I., BROWN, C.V. & MCHALE, G. 2016 Not spreading in reverse: the dewetting of a liquid film into a single drop. *Sci. Adv.* **2** (9), e1600183.

DE GENNES, P.G. 1985 Wetting: statics and dynamics. *Rev. Mod. Phys.* **57**, 827–863.

DE GENNES, P.-G., BROCHARD-WYART, F. & QUÉRÉ, D. 2004 *Capillarity and Wetting Phenomena: Drops, Bubbles, Pearls, Waves*, vol. 315. Springer.

GOKHALE, S.J., DASGUPTA, S., PLAWSKY, J.L. & WAYNER, P.C. 2004 Reflectivity-based evaluation of the coalescence of two condensing drops and shape evolution of the coalesced drop. *Phys. Rev.* E **70** (5), 051610.

GONG, X.J., GAO, X.F. & JIANG, L. 2017 Recent progress in bionic condensate microdrop self-propelling surfaces. *Adv. Mater.* **29** (45), 14.

GOOSSENS, S., SEVENO, D., RIOBOO, R., VAILLANT, A., CONTI, J. & DE CONINCK, J. 2011 Can we predict the spreading of a two-liquid system from the spreading of the corresponding liquid-air systems? *Langmuir* **27** (16), 9866–9872.

HERNANDEZ-SANCHEZ, J.F., LUBBERS, L.A., EDDI, A. & SNOEIJER, J.H. 2012 Symmetric and asymmetric coalescence of drops on a substrate. *Phys. Rev. Lett.* **109** (18), 184502.

HUANG, K.-L. & PAN, K.-L. 2021 Transitions of bouncing and coalescence in binary droplet collisions. *J. Fluid Mech.* **928**, A7.

IQBAL, R., DHIMAN, S., SEN, A.K. & SHEN, A.Q. 2017 Dynamics of a water droplet over a sessile oil droplet: compound droplets satisfying a Neumann condition. *Langmuir* **33** (23), 5713–5723.

JI, B., YANG, Z. & FENG, J. 2021 Compound jetting from bubble bursting at an air-oil-water interface. *Nat. Commun.* **12** (1), 6305.

JIANG, X., ZHAO, B. & CHEN, L. 2019 Sessile microdrop coalescence on partial wetting surfaces: effects of surface wettability and stiffness. *Langmuir* **35** (40), 12955–12961.

KAMP, J., VILLWOCK, J. & KRAUME, M. 2017 Drop coalescence in technical liquid/liquid applications: a review on experimental techniques and modeling approaches. *Rev. Chem. Engng* **33** (1), 1–47.

KARPITSCHKA, S. & RIEGLER, H. 2010 Quantitative experimental study on the transition between fast and delayed coalescence of sessile droplets with different but completely miscible liquids. *Langmuir* **26** (14), 11823–11829.

KEISER, A., KEISER, L., CLANET, C. & QUÉRÉ, D. 2017 Drop friction on liquid-infused materials. *Soft Matt.* **13** (39), 6981–6987.

KHATTAB, I., BANDARKAR, F., ABOLGHASSEMI FAKHREE, M.A. & JOUYBAN, A. 2012 Density, viscosity, and surface tension of water + ethanol mixtures from 293 to 323 K. *Korean J. Chem. Engng* **29**, 812–817.

KHISMATULLIN, D.B. & NADIM, A. 2001 Shape oscillations of a viscoelastic drop. *Phys. Rev.* E **63** (6), 061508.

KOLDEWEIJ, R.B.J., VAN CAPELLEVEEN, B.F., LOHSE, D. & VISSER, C.W. 2019 Marangoni-driven spreading of miscible liquids in the binary pendant drop geometry. *Soft Matt.* **15**, 8525–8531.

KUSUMAATMAJA, H., MAY, A.I. & KNORR, R.L. 2021 Intracellular wetting mediates contacts between liquid compartments and membrane-bound organelles. *J. Cell Biol.* **220** (10), e202103175.

LAMB, H. 1924 *Hydrodynamics*. Cambridge University Press.

Lee, M.W., Kim, N.Y., Chandra, S. & Yoon, S.S. 2013 Coalescence of sessile droplets of varying viscosities for line printing. *Intl J. Multiphase Flow* **56**, 138–148.

Li, X., Li, S., Lu, Y., Liu, M., Li, F., Yang, H., Tang, S.-Y., Zhang, S., Li, W. & Sun, L. 2020 Programmable digital liquid metal droplets in reconfigurable magnetic fields. *ACS Appl. Mater. Interfaces* **12** (33), 37670–37679.

Lu, L.L., Pei, Y.Q., Qin, J., Peng, Z.J., Wang, Y.Q. & Zhu, Q.Y. 2020 Impingement behaviour of single ethanol droplet on a liquid film of glycerol solution. *Fuel* **276**, 117820.

Mahadevan, L., Adda-Bedia, M. & Pomeau, Y. 2002 Four-phase merging in sessile compound drops. *J. Fluid Mech.* **451**, 411–420.

Menchaca-Rocha, A., Martínez-Dávalos, A., Núñez, R., Popinet, S. & Zaleski, S. 2001 Coalescence of liquid drops by surface tension. *Phys. Rev.* E **63** (4), 046309.

Narhe, R., Beysens, D. & Nikolayev, V.S. 2004 Contact line dynamics in drop coalescence and spreading. *Langmuir* **20** (4), 1213–1221.

Narhe, R.D., Beysens, D.A. & Pomeau, Y. 2008 Dynamic drying in the early-stage coalescence of droplets sitting on a plate. *Europhys. Lett.* **81** (4), 46002.

Neogi, P. & Miller, C.A. 1982 Spreading kinetics of a drop on a smooth solid surface. *J. Colloid Interface Sci.* **86** (2), 525–538.

Paulsen, J.D. 2013 Approach and coalescence of liquid drops in air. *Phys. Rev.* E **88** (6), 063010.

Pawar, N., Bahga, S., Kale, S. & Kondaraju, S. 2019*a* Symmetric and asymmetric coalescence of droplets on a solid surface in the inertia-dominated regime. *Phys. Fluids* **31**, 092106.

Pawar, N.D., Bahga, S.S., Kale, S.R. & Kondaraju, S. 2019*b* Symmetric and asymmetric coalescence of droplets on a solid surface in the inertia-dominated regime. *Phys. Fluids* **31** (9), 092106.

Ristenpart, W.D., McCalla, P.M., Roy, R.V. & Stone, H.A. 2006 Coalescence of spreading droplets on a wettable substrate. *Phys. Rev. Lett.* **97** (6), 064501.

Rostami, P. & Auernhammer, G.K. 2022 Capillary filling in drop merging: dynamics of the four-phase contact point. *Phys. Fluids* **34** (1), 012107.

Sanjay, V., Sen, U., Kant, P. & Lohse, D. 2022 Taylor–Culick retractions and the influence of the surroundings. *J. Fluid Mech.* **948**, A14.

Shyam, S., Dhapola, B. & Mondal, P.K. 2022 Magnetofluidic-based controlled droplet breakup: effect of non-uniform force field. *J. Fluid Mech.* **944**, A51.

Siahcheshm, P., Goharpey, F. & Foudazi, R. 2018 Droplet retraction in the presence of nanoparticles with different surface modifications. *Rheol. Acta* **57** (11), 729–743.

Sohrabi, S., Kassir, N. & Keshavarz Moraveji, M. 2020 Droplet microfluidics: fundamentals and its advanced applications. *RSC Adv.* **10** (46), 27560–27574.

Somwanshi, P.M., Muralidhar, K. & Khandekar, S. 2017 Wall shear rates generated during coalescence of pendant and sessile drops. In *Fluid Mechanics and Fluid Power – Contemporary Research* (ed. A.K. Saha, D. Das, R. Srivastava, P.K. Panigrahi & K. Muralidhar), pp. 33–42. Springer.

Somwanshi, P.M., Muralidhar, K. & Khandekar, S. 2018 Coalescence dynamics of sessile and pendant liquid drops placed on a hydrophobic surface. *Phys. Fluids* **30** (9), 092103.

Song, H., Chen, D.L. & Ismagilov, R.F. 2006 Reactions in droplets in microfluidic channels. *Angew. Chem. Intl Ed. Engl.* **45** (44), 7336–7356.

Sprittles, J.E. & Shikhmurzaev, Y.D. 2014 Dynamics of liquid drops coalescing in the inertial regime. *Phys. Rev.* E **89**, 063008.

Sui, Y., Maglio, M., Spelt, P.D.M., Legendre, D. & Ding, H. 2013 Inertial coalescence of droplets on a partially wetting substrate. *Phys. Fluids* **25** (10), 101701.

Sykes, T.C., Castrejón-Pita, A.A., Castrejón-Pita, J.R., Harbottle, D., Khatir, Z., Thompson, H.M. & Wilson, M.C.T. 2020*a* Surface jets and internal mixing during the coalescence of impacting and sessile droplets. *Phys. Rev. Fluids* **5** (2), 023602.

Sykes, T.C., Harbottle, D., Khatir, Z., Thompson, H.M. & Wilson, M.C.T. 2020*b* Substrate wettability influences internal jet formation and mixing during droplet coalescence. *Langmuir* **36** (32), 9596–9607.

Thoroddsen, S.T., Qian, B., Etoh, T.G. & Takehara, K. 2007 The initial coalescence of miscible drops. *Phys. Fluids* **19** (7), 072110.

Wang, X., Xu, B., Chen, Z., Del Col, D., Li, D., Zhang, L., Mou, X., Liu, Q., Yang, Y. & Cao, Q. 2022 Review of droplet dynamics and dropwise condensation enhancement: theory, experiments and applications. *Adv. Colloid Interface Sci.* **305**, 102684.

Winkelmann, M., Grimm, E.-M., Comunian, T., Freudig, B., Zhou, Y., Gerlinger, W., Sachweh, B. & Petra Schuchmann, H. 2013 Controlled droplet coalescence in miniemulsions to synthesize zinc oxide nanoparticles by precipitation. *Chem. Engng Sci.* **92**, 126–133.

XIE, H., ZHAO, W., ZHANG, X. & WANG, Z. 2022 Demulsification of bacteria-stabilized pickering emulsions using modified silica nanoparticles. *ACS Appl. Mater. Interfaces* **14** (21), 24102–24112.

XU, H., WANG, T. & CHE, Z. 2022 Bridge evolution during the coalescence of immiscible droplets. *J. Colloid Interface Sci.* **628**, 869–877.

YOKOTA, M. & OKUMURA, K. 2011 Dimensional crossover in the coalescence dynamics of viscous drops confined in between two plates. *Proc. Natl Acad. Sci. USA* **108** (16), 6395–6398.

YU, H., KANT, P., DYETT, B., LOHSE, D. & ZHANG, X. 2019 Splitting droplets through coalescence of two different three-phase contact lines. *Soft Matt.* **15** (30), 6055–6061.

YUAN, B., HE, Z., FANG, W., BAO, X. & LIU, J. 2015 Liquid metal spring: oscillating coalescence and ejection of contacting liquid metal droplets. *Sci. Bull.* **60** (6), 648–653.

ZHANG, Y., OBERDICK, S.D., SWANSON, E.R., ANNA, S.L. & GAROFF, S. 2015 Gravity driven current during the coalescence of two sessile drops. *Phys. Fluids* **27** (2), 022101.

ZHAO, H., OREJON, D., SEFIANE, K. & SHANAHAN, M.E.R. 2021 Droplet motion and oscillation on contrasting micro-striated surfaces. *J. Fluid Mech.* **916**, A54.